ONLINE FIRST July 2, 2024

Engineering Transactions, **72**, doi: 10.24423/EngTrans.2024.3281
Institute of Fundamental Technological Research Polish Academy of Sciences (IPPT PAN)
Université de Lorraine • Poznan University of Technology

Research Paper

Impact of Trace Amounts of Sc and Zr on the Tribological Performance of Al-Bronze Against Stainless Steel Counterface in Varying Conditions

Mohammad Salim KAISER

Innovation Centre, International University of Business Agriculture and Technology
Dhaka-1230, Bangladesh; e-mail: dkaiser.res@iubat.edu

The influence of trace amounts of scandium (Sc) and zirconium (Zr) on the tribological behavior of aluminum (Al)-bronze has been studied under ambient conditions in various sliding environments, including dry conditions, fresh water, and simulated seawater. The findings demonstrate that trace amounts of Sc and Zr significantly influence wear properties, improving Al-bronze performance in dry sliding conditions while diminishing it in wet and corrosive environments. The addition of Sc and Zr refines the grains, increases the thermal stability of Al-bronze through intermetallic formation, and is simultaneously affected by oxidation and corrosion. Scandium increases the intensity of these effects, as intermetallic compounds strengthen the alloy but also accelerate the corrosion process.

Keywords: Cu-alloy; friction; microstructure; wear rate; worn surfaces.

1. Introduction

In general, copper is a soft, ductile, and highly conductive material both thermally and electrically in its pure state [1–3]. Al-bronze is one of the most important alloys among more than four hundred distinct copper alloys because it has excellent casting and welding properties, high strength, toughness, and wear resistance, as well as outstanding corrosion resistance. Aluminum, which ranges from more or less 6 to 12%, is utilized as the primary alloying element instead of tin, which is often used in other forms of bronze [4, 5]. The base element, copper, makes up the remaining portion; however, additional substances such as zinc, nickel, iron, or silicon may be added to improve the metal's qualities [6, 7]. In addition, to improve the properties, a limited number of copper (Cu)-based alloys can be reinforced through cold working, thermal treatment, and solid-solution alloying. The properties of Al-bronze can be improved via all the above processes [8, 9].

Groups of alloys are formed from aluminum bronzes, which vary based on the proportion of aluminum and other elements in the metal [10]. Alloying elements are used as major, minor, modifiers, and impurity elements. It is well established that Zr, as a grain refiner, plays a great role in Cu-alloys, improving the overall structural as well as mechanical properties. Similarly, Sc not only refines the grain structure but also participates in enhancing precipitation strengthening [11, 12]. The strength and corrosion resistance of Al-bronze have made it popular in the energy, chemical, and marine industries. This type of Cu-alloy is used for making bushes, gear, and different moveable parts, so the wear properties of this material are very important [13]. This is due to its superior resistance to wear and corrosion, high electrical and thermal conductivity, and capacity for self-lubrication. Wear is the overall material loss from a surface due to mechanical processes such as contact with liquid, solid, or gaseous objects, or relative motion between objects. It occurs by the separation of wear debris-forming particles and the plastic displacement of surface materials, where the sizes of the particles vary from millimeters to nanometers [14, 15]. Wear can change over time or as a result of changing operational conditions. Frictional heating typically accelerates wear through mechanical and chemical reactions. To describe wear mechanisms, a wide variety of terms are used, such as adhesive, abrasive, fretting, surface fatigue, corrosion, and erosion[16].

The use of this alloy continuously increases. As a result, there is an ongoing need to enhance the efficiency of its manufacturing processes, and significant trends are progressively advancing a variety of research areas. As new technical applications arise, there is an increasing demand for stronger materials with improved qualities. The material is recycled and used again when a product reaches the end of its useful life. Cu-alloys are particularly popular materials since their quality does not significantly deteriorate when they are reused. Recycling these materials has significant benefits in reducing environmental pollutants and energy consumption [17, 18]. Trace additions can then be made easily. Additionally, melting parameters can be adjusted to obtain the desired properties for these alloys.

The impact of trace levels of Sc and Zr on both the physical and mechanical characteristics of Cu-based Al-bronze has been studied extensively. It is well-known that even small additions cause changes to alloy properties. Obviously, any improvements in one property can lead to changes in other alloy properties. While Sc and Zr have a positive effect on the strength and microstructure of Al-bronze, there are not enough reports on the wear and friction behavior of this alloy with their additions. As it is commonly used material for gears, the primary goal of this study is to assess how well this alloy performs in various sliding environments, including corrosive, wet, and dry environments. A pin-on-disk wear testing method is employed, since it is a standard screening method for assess-

ing the tribological performance of any material. Consequently, a comparison of wear rates alongside coefficients of friction is conducted as part of this study.

2. Experimental methods

This study focused on a Cu-10 wt% Al alloy, known as Al-bronze, with additions of 0.2 wt% Sc and 0.2 wt% Zr. Pure copper and commercially available aluminum were used in the production of Al-bronze. Specifically, master alloys Al-2 wt% Sc and Al-10 wt% Zr were used for other bronze alloys. The melting process was conducted in a pit furnace that used natural gas as fuel and had clay graphite crucibles. A suitable flux or degasser was used during this process. The furnace melting temperature was maintained constant, like $1300 \pm 15°C$. A steel mold of size $20 \times 100 \times 150$ mm coated with water clay was prepared and preheated to 200°C. The melts were homogenized at 1200°C with stirring and then poured into the mold. The chemical compositions of the three categories of Al-bronzes were determined by means of spectrochemical analysis. The main constituents were measured at five points on the sample surfaces, and the mean values are displayed in Table 1. Furthermore, the alloys contained trace amounts of Zn, Pb, Sn, Ni, Mn, Cr, Sb, etc.

Table 1. Chemical composition by wt% of three categories of Al-bronzes.

Alloy	Al	Sc	Zr	Fe	Fe	Si	Cu
Cu-Al	9.601	0.000	0.000	0.078	0.078	0.004	Bal
Cu-Al-Sc	9.451	0.198	0.000	0.156	0.156	0.002	Bal
Cu-Al-Zr	9.470	0.000	0.189	0.064	0.064	0.005	Bal

The oxide layer formed on the surfaces of Cu-Al, Cu-Al-Sc, and Cu-Al-Zr alloys during casting was removed using a shaper machine. Cast alloys were cold rolled with 50% reduction in a rolling mill with a 10 HP capacity. The alloys were cut into dimensions of 20 mm × 20 mm × 150 mm, and approximately 1 mm deformation was applied per pass. Cold rolling reduced the thickness from 20 mm to 10 mm. Samples measuring 10 mm × 20 mm × 20 mm were made from cold-rolled alloys, and all three alloys were isochronally aged for two hours at various temperatures. The samples were mechanically sanded with 1500 grit emery paper, both rough and fine. Microhardness of the aged samples was assessed using a Micro Vickers Hardness Tester, applying 1 kg load with a Knoop indenter for 10 seconds. At least eleven indentations were made on each sample from different angles, and average values were used to plot the data. A pin-type sample was machined for the wear investigation from all three cold-rolled alloys. The sample measured five millimeters in diameter and fourteen millimeters in length. In order to achieve highest hardness, all three samples were homogenized through

artificially ageing at a temperature of 300°C for two hours, consistent with previous studies [8]. The pin sample's ends (5 mm in diameter) were polished with 1500-grit emery papers. Next, running water was used to clean the end surfaces.

Finally, acetone was used to dry the samples. Discs made of 309s grade stainless steel were used as the counter body. The surfaces of the discs were polished using a surface grinding machine and cleaned with acetone and cotton. The discs were HRB 85 in hardness. The disc's surface roughness (center line average roughness, Ra) was 0.40 μm. Conversely, the surface roughness of the polished pin sample, containing Al-bronze, trace amounts of Sc and Zr, w measured to be 0.23, 0.21, and 0.23 μm, respectively. The tribological behaviors of the three alloys were studied using a pin-on-disc type wear apparatus following the standard ASTM G99-05 [19]. During the wear tests, the end surface of the pin samples was pressed against a stainless-steel disc that rotated horizontally. Generally, Cu-based gear material does not perform so well under heavy loads compared to ferrous metals. To maintain consistency with previous studies, a constant applied load of 20 N was used throughout the entire test, resulting in nominal contact pressures of 1.02 MPa [20–22].

For other tests, applied loads ranging from 5 to 50 N were used. The experiments were conducted using different sliding distances, which ranged from 100 m to 3000 m, with a sliding velocity of 0.385 m/s. All tests were carried out at an ambient air temperature of 23°C with a relative humidity of 65% in dry conditions, wet conditions, distilled water, and 3.5% NaCl solution environment. The 3.5% NaCl solution, simulating seawater, was prepared by dissolving sodium chloride reagent powder in deionized water. Since seawater contains about 3.5% of NaCl, this obtained solution was similar to natural seawater composition [23]. During the experiments, a single point of drip-type lubrication was maintained at the contact interface between the sample and the stainless-steel counter plate in both distilled water and NaCl solution environments. A discharge rate was five drops per minute, as controlled by a regulator. Other parameters were identical to those in the dry wear test. For each type of material, at least nine tests were conducted. The average values of the weight-loss measurements following each test were used to calculate wear rates. The track diameter and rotational speed of the stainless-steel disc were 49 mm and 150 rpm, respectively, and were used to calculate the sliding distance. After each test, caution was taken to prevent wear debris from becoming entrapped.

Wear rates and friction coefficients were computed using the following formulas [24]:

$$\Delta W = W_{\text{initial}} - W_{\text{final}}, \tag{2.1}$$

$$\text{S.W.R.} = \frac{\Delta W}{\text{S.D.} \times L}, \tag{2.2}$$

$$\mu = \frac{F}{L}, \tag{2.3}$$

where W_{initial} – sample weight before wear, g; W_{final} – sample weight after wear, g; ΔW – the weight loss of the sample during wear, g; S.D. – sliding distance during wear, m; L – applied load, N; S.W.R. – specific wear rate, g/Nm; μ – friction coefficient and; F – frictional force, N.

The samples underwent optical metallography in the standard procedure. When using copper etching in metallography, a commonly recommended mixture of ammonium hydroxide and three percent hydrogen peroxide in a 1:1 ratio was applied. The cleaned and dried samples were examined at various magnifications using a Unitron Versamet-2 optical microscope, and selected photomicrographs were taken. A JEOL scanning electron microscope (SEM) was employed for analysis of the worn surfaces. A Taylor Hobson Surtronic S-100 Roughness Tester was used to measure the roughness of the worn surfaces in various sliding environments. Figure 1 depicts the configuration of the wear testing apparatus, wear specimen, and counter body, all comprising the experimental setup.

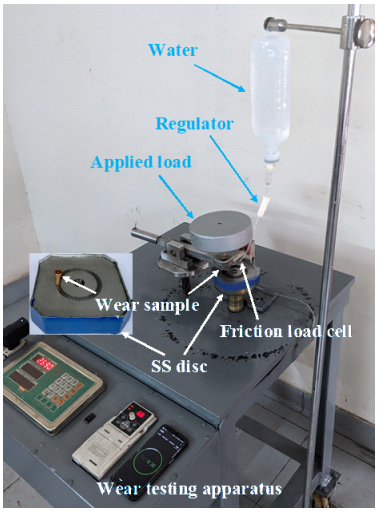

FIG. 1. Depiction of the experimental setup including the wear testing machine, wear specimen and counter body.

3. Results and discussion

3.1. Isochronal ageing

Figure 2 demonstrates the hardness variation of 50% cold-rolled Al-bronze alloys with added trace amounts of Sc and Zr after two hours of isochronal ageing. All alloys exhibit similar ageing behavior, where an initial increase occurs

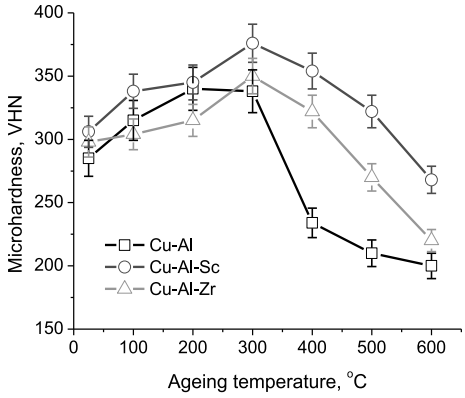

FIG. 2. Microhardness of 50% cold-rolled three alloys after two hours of isochronal ageing.

to a certain point, followed by a rapid decrease at varying rates. During the initial ageing stage, two processes happen: the formation of Guinier–Preston zones related to the early stages of precipitation in the alloy leading to increased hardness, and stress relief in cold-deformed alloys resulting in a hardness decrease. Here, the average of these two competing effects is represented in the graph; the first effect is greater than the second, thereby improving the microhardness. Additionally, Fig. 2 demonstrates that the hardness of three alloys reaches its highest level at the ageing temperature of 300°C. These results indicate that the inclusion of Al contributes significantly to the alloy's age hardening effect.

During solidification and ageing, Al and Cu undergo reactions leading to the formation of various intermetallic phases, such as $CuAl_2$, AlCu, Cu_4Al_3, Cu_3Al_2, or Al_4Cu_9. Among these phases, Al_4Cu_9 and Cu_3Al_2 are particularly notable for their significant effect on enhancing the alloy's hardness [25, 26]. The drastic decrease in hardness beyond the ageing temperature of 300°C can be attributed to precipitation coarsening, recovery, and recrystallization, altogether known as the over-ageing effect.

In contrast, alloys with trace additions of Sc and Zr initially display superior hardness due to their relatively fine grain compared to Al-bronze. During solidification, Sc and Zr act as nucleation sites, influencing grain structure formation. Moreover, these trace elements show lower ageing response rates initially and reduced softening at higher ageing temperatures. During solidification and ageing treatment, Sc and Zr added to Al-bronze form dispersoid particles of Al_3Sc and Al_3Zr with Al, respectively. In addition, Cu forms intermetallics such as Cu_4Sc, Cu_2Sc and CuSc when combined with Sc. Likewise, doping with Zr results in the formation of Cu_9Zr_2 intermetallic compound [27, 28]. These precipitates prevent the alloy's precipitation coarsening and effectively block dislocation motion. As a result, processes like hardness improvement and recrystallization are delayed.

One thing that can be noticed is that the intermetallics of Sc are hard particles; thus, they always accelerate the hardness of Al-bronze alloys.

3.2. Wear behavior

The average weight loss variation with sliding distance in each of the nine tests of Al-bronze and Al-bronze with trace additions of Sc and Zr are shown in Fig. 3. Pressure and velocity were set at 1.02 MPa and 0.385 m/s, respectively, under dry sliding conditions. The usual phenomenon of weight loss with increasing sliding distance is observed for all samples, but its intensity varies. Throughout the test, as the sliding distance increases, the contact period between the rotating disk and the sample face also increases, resulting in further weight loss. The variation in results is associated with material properties such as hardness, density, softening behavior, etc. [29].

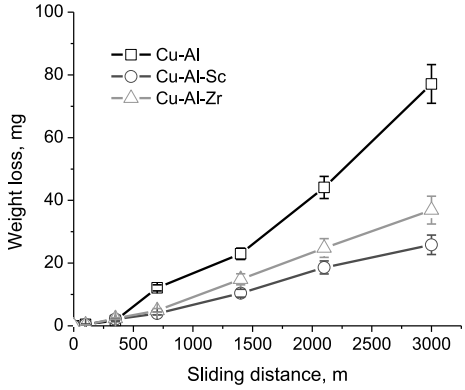

FIG. 3. Weight loss variation with sliding distance in a dry sliding environment with a velocity of 0.385 m/s and pressure of 1.02 MPa.

Using Eqs. (2.1) and (2.2), the calculated wear rates of the above-mentioned three investigated alloys are plotted against sliding distance in Figs. 4–6, showing the difference in wear rates under dry, wet, and corrosive (3.5% NaCl) environments, respectively. From Fig. 4, it is observed that under dry sliding conditions, the wear rate initially increases with sliding distance, followed by a tendency towards a constant value. This elevated wear rate can be attributed to the generation of frictional heat under high pressure, which results in extended close contact between the mating surfaces and material softening [30], thereby increasing wear. Notably, Al-bronze exhibits higher wear rate compared to the trace-added alloys, with Zr addition improving thermal stability. The addition of Sc not only improves thermal stability but also participates in precipitation strengthening, demonstrating the best wear resistance. Archard's theory on wear and its relation to the hardness of materials is consistent with the observed behavior of

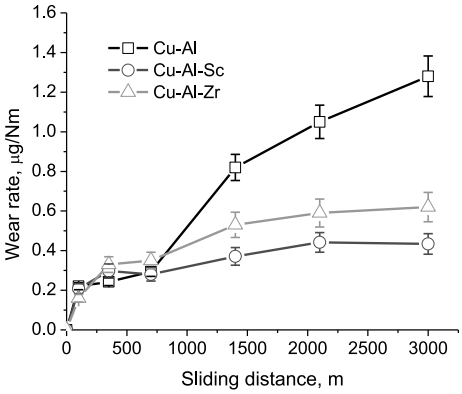

FIG. 4. Wear rate variation with sliding distance in a dry sliding environment with a velocity of 0.385 m/s and pressure of 1.02 MPa pressure.

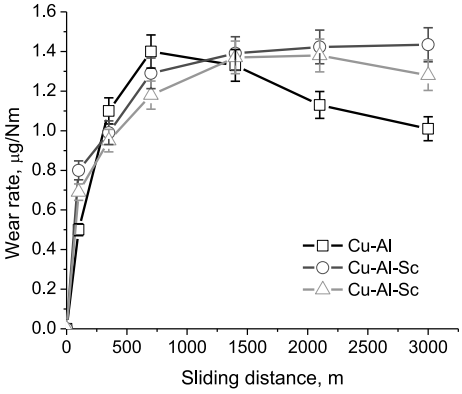

FIG. 5. Wear rate variation with sliding distance in a wet sliding environment with a velocity of 0.385 m/s and pressure of 1.02 MPa.

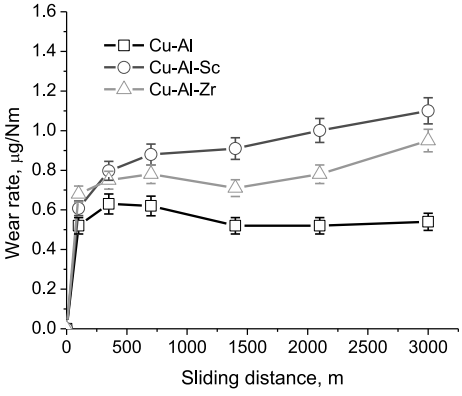

FIG. 6. Wear rate variation with sliding distance in a corrosive sliding environment with a velocity of 0.385 m/s and pressure 1.02 MPa.

aluminum bronze alloys in dry sliding conditions, as the wear rate of alloys in dry sliding conditions decreases as hardness increases [31]. In addition, one of the likely causes of the lower wear rate is the formation of an intermediate oxide film between mating surfaces during wear tests. The average values of these two opposite effects are displayed in the graphs. For long-term sliding contact, the surfaces exposed to air form thick oxide layers. These layers can control the wear rate and help maintain a constant wear rate [24].

Under distilled water sliding condition, the wear rate significantly increases for all alloys (Fig. 5). Throughout sliding, water promotes oxidation on the surfaces, leading to continuous dissolution or uniform. The trace-added alloy, with its fine grains, forms higher oxides, resulting in a slightly higher wear rate. More specifically, the grains containing impurities and different foreign particles are rapidly affected by oxidation [32].

A fully opposite phenomenon in alloy wear rates to that in dry sliding conditions is observed for corrosive sliding in a 3.5% NaCl environment. The wear exhibits an increase and stabilizes with sliding distance, where trace-added bronzes show higher wear rates (Fig. 6). Clearly, this is due to corrosive wear, where adding a trace amounts of Sc to Al-bronze, accelerates wear in the corrosive environment, followed by Zr-added bronze. It is known that the higher grain boundary are more susceptible to corrosion or oxidation [33]. During friction, usually a higher level of corrosive products accumulates on the edges. However, the dissolution rate of these corrosive products is higher in the case of Sc compared to Zr [34]. It may be noted that corrosive products are more stable on surfaces in the absence of water, resulting in a lower wear rate compared to when these products form oxides in a wet environment [35].

The intensity of the average friction coefficients under dry, wet, and corrosive tested environments of all discussed alloys with different sliding distances is shown in Figs. 7–9. In all cases, the friction coefficient is initially low, increases with sliding distance, and then stabilizes at relatively constant values. The friction coefficient values are initially low due to the contact between oxide films on the specimen surface and the disc material. Within a short sliding distance, the friction coefficient increases. This is due to the fact that metal-to-metal contact causes the surface oxide layer to crack and be removed, increasing the coefficient of friction. With increasing sliding distance, interface temperatures can develop, which can promote surface oxidation, thereby reducing direct surface contact and slightly reducing the friction coefficient [36].

The presence of a wet and corrosive environment can significantly reduce the coefficient of friction compared to a dry environment, primarily due to the sealing effect lessening the roughness of the surfaces in contact [37]. It can be noted that the behavior of alloys with added traces is somewhat different with respect to the coefficient of friction in wet environments. The thermal stability of these

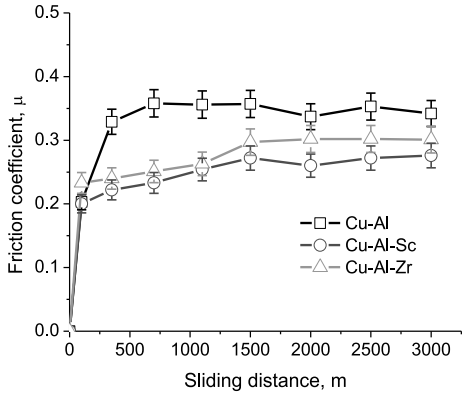

FIG. 7. Friction coefficient variation with sliding distance in a dry sliding environment with a velocity of 0.385 m/s and pressure of 1.02 MPa.

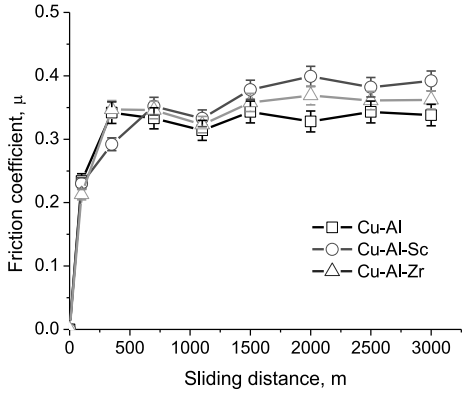

FIG. 8. Friction coefficient variation with sliding distance in a wet sliding environment with a velocity of 0.385 m/s and pressure of 1.02 MPa.

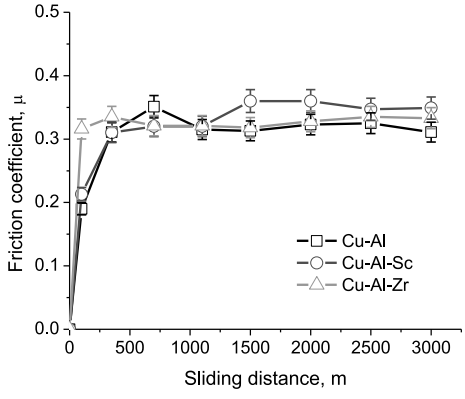

FIG. 9. Friction coefficient variation with sliding distance in a corrosive sliding environment with a velocity of 0.385 m/s and pressure of 1.02 MPa pressure.

alloys is compromised under wet sliding conditions due to the resistance to dissipate heat generated between the contact surfaces Additionally, soft and quickly removed oxide layers form on the surface, contributing to the high wear rates in trace-added alloys under wet sliding conditions. Aluminum bronze has the highest coefficient of friction in a dry sliding environment because the results are in good agreement with the alloys' measured microhardness values. Deficits in the friction coefficient may be caused by variations in the degree of localized plastic deformation at actual contact areas. The trace Zr-added bronze exhibits a lower friction coefficient, while Sc-added bronze has the lowest friction as it is the hardest one and undergoes the lowest plastic deformation [38]. The coefficient of friction in wet and corrosive environments depends on the formation of the oxide layer as well as the corrosive product, and the resulting hardness is not the controlling factor for friction. The minimal variations in the friction coefficients amongst the alloys prove this.

For all three alloys, the average friction coefficient under different contact pressures and environments at a constant speed of 0.385 m/s is presented in Figs. 10, 11, and 12. In dry sliding conditions, the friction coefficient typically exhibits a decreasing trend, due to the formation of oxide layers (Fig. 10). Although there may be some deflection with increasing pressure, stress, and temperature, these factors also increase and soften the materials. As the materials soften and undergo greater plastic deformation beyond a certain pressure, the coefficient increases. This trend is less pronounced for trace-added alloys due to their thermal stability. However, under wet sliding condition, all samples show decreasing trends in the coefficient of friction with increasing applied pressures (Fig. 11). In this case, higher pressures produce some oxide layer due to the presence of water, which inhibits heat generation as a result of lower friction. The oxide layer formation of the individual alloys, along with sealing effects,

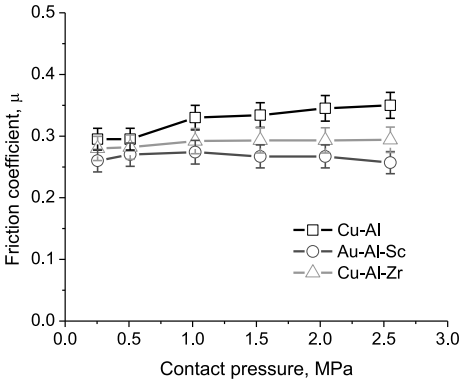

FIG. 10. Characteristics of the coefficient of friction in a dry sliding environment under contact pressure.

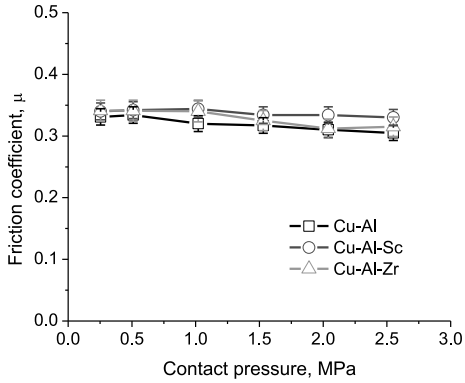

FIG. 11. Characteristics of the coefficient of friction in a wet sliding environment under contact pressure.

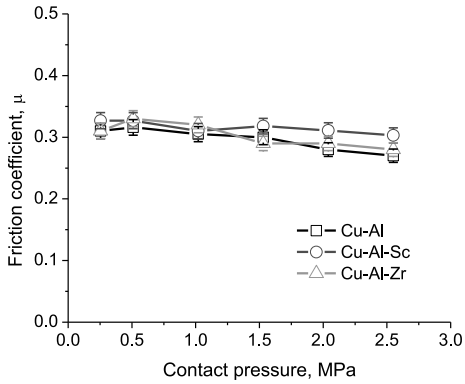

FIG. 12. Characteristics of the coefficient of friction in a corrosive sliding environment under contact pressure.

reduces these coefficients. Additionally, under corrosive condition, the friction coefficient is fully controlled by saline water (Fig. 12). Most alloys exhibit similar friction coefficient levels. A higher oxide layer is formed in the trace-added bronzes due to their fine grain, and as a result, the removal of the continuous oxide layer is higher. As a result, some deviation is observed [39, 40].

3.3. Optical micrographs

The worn surfaces of three Al-bronzes under different experimental conditions, including wear before and after dry, wet, and the NaCl corrosive sliding environment, are presented in Fig. 13. The experiments were conducted at a pressure of 1.02 MPa, with a 0.385 m/s sliding velocity and a 3000 m sliding distance. Before wear testing, the polished surfaces exhibited a moderately smooth surface

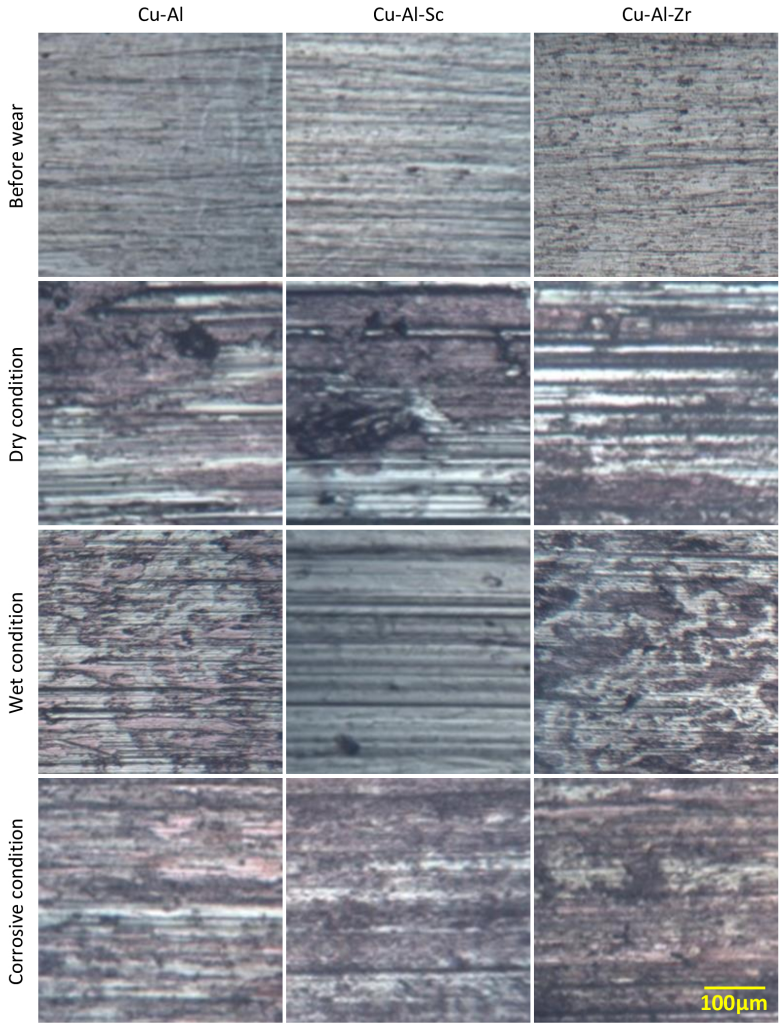

FIG. 13. Optical micrographs of experimental alloy surfaces before wear and after wear under dry, wet and corrosive sliding conditions, with a distance of 3000 m and pressure of and 1.02 MPa.

texture without any signs of plastic deformation or scratches. During polishing, metallographic emery paper created some scatter marks throughout in one direction. However, this type of smooth polished surface without etching did not reveal information about the microstructure. Only different shades indicated different levels of alloying elements in the alloys. Al-bronze exhibited different white elongated shade areas, indicating the presence of Al phase in the Cu matrix. In contrast, Sc and Zr-added bronzes, exhibited finely and uniformly distributed, reflecting their refined grains [12, 32].

Furthermore, plastic deformation and numerous prominent cracks are observed on the worn surfaces under dry sliding conditions. A significant amount of material is observed to be delaminated. It can also be observed from the figure that polished marks on the worn surfaces are fully absent, indicating that delamination occurred by removing particles. In comparison to Al-bronze, the worn surface of the Sc and Zr trace-added alloy exhibits a surface morphology with fewer cracks and shallow grooves. The trace added alloys consist of a fine grain structure with better strength. The signs of wear and fragments illustrate the mechanisms of wear by oxidation, delamination, and abrasive wear [32].

In contrast, wear tracks visible on the worn surface exposed to a wet environment appear relatively smooth. Hardly any cracks are visible. In addition, hardly any cracks are visible, and debris and grooves are sparse. Additionally, because of liquid environment's cooling and lubricating properties, some dark areas can be seen. The liquid environment prevents the formation of cracks and debris by lowering local stress, heat concentration, and shear friction. Additionally, most particles and debris are washed away by water during the sliding process, reducing abrasive wear. As a result, the liquid environment's frictional characteristics are much better than those of the surrounding air. However, in the 3.5% NaCl saline environment, the wear mechanism is altered. The oxide film is actually created by corrosion wear that occurs in the corrosive solution. During the wear testing, oxides are subsequently broken down, producing wear debris. Additionally, heat from the friction produced at the interface prompts the growth of more oxides, as confirmed by changes in surface color. The debris and particle sizes are smaller than those created through dry sliding conditions, and there are no signs of cracks or plastic deformation [41].

The dust particles produced during the wear test of all three Al-bronzes in a dry sliding environment are displayed in Fig. 14. The same pressure of 1.02 MPa and sliding velocity of 0.385 m/s were applied during this procedure. There is granular alloy dust and stainless-steel discs in some of the chips.

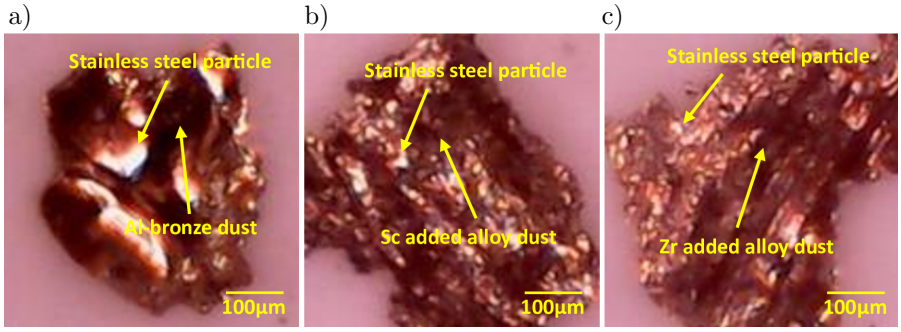

FIG. 14. Snapshots of dust generated from wear under dry sliding conditions: a) Al-bronze, b) trace Sc-added Al-bronze, c) trace Zr-added Al-bronze.

The amount of steel chips in the dust varies depending on the alloys. Due to its lower hardness, aluminum bronze dust contains comparatively few stainless-steel chips. Sc-containing alloy dust consists of the highest amount of stainless-steel chips, followed by Zr-containing alloy dust, due to their maximum and highest hardness respectively. Additionally, the size of chips made by Al-bronze is the largest, while those made by bronze with Zr is the smallest, followed by bronze with Sc. This can be explained by the grain size of Al-bronzes. Zirconium introduces fine precipitates compared to Sc and refined grain structures in the alloy. An example is fine grinding wheels that produce fine particles during grinding, which affect the size of the counter body particles [42].

Figure 15 depicts the optical microstructures of 50% cold-rolled Al-bronzes without and with trace Sc and Zr additions. Those alloys were aged at 300°C for two hours. Usually aging at this temperature does not change the grain orientation of such alloys. Some stress relief can occur and form various precipitates within the alloys. The distorted grains caused by cold rolling are clearly visible in all microstructures, along with the elongated grains in the rolling direction. It is well known that the microstructure of Al-bronze is composed of numerous intermetallic K-phases, including α-phase, β-phase, or retained martensitic β'-phase (Fig. 15a). The four main categories of K-phases are κI, κII, κIII and κIV. In the alloy microstructure, K-phases with the chemical compositions of Cu, Al, Fe, and Ni can appear in various arrangements. With the addition of trace elements, it is apparent that the alloy's dendrite arm spacing is reduced, leading to dendrite refinement (Figs. 15b and 15c). As the dendrite structure of the alloy grows, Sc and Zr modify the solidification speed during casting [43, 44]. Trace-added alloy microstructures demonstrate that the grain refining effect of Zr alone is superior to that of Sc. A similar observation was previously made that the atomic size and diffusion coefficient of Zr are lower than those of Sc [45].

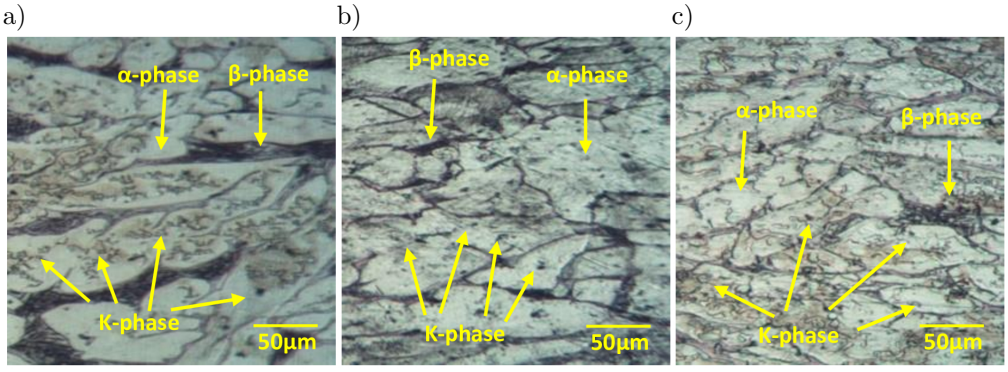

FIG. 15. Optical micrograph of Al.-bronzes subjected to 50% deformation and aged at 300°C for two hours: a) Al-bronze, b) trace Sc-added Al-bronze, c) trace Zr-added Al-bronze.

3.4. Scanning electron microscopy

Through SEM, worn surfaces of the discussed three types of Al-bronzes are shown following the wear test in dry sliding conditions over a distance of 3000 m. The same pressure of1.02 MPa and sliding velocity of 0.385 m/s were used during the wear study. In Fig. 16, images at higher magnifications are also displayed accordingly for better understanding. The images distinctly indicate grooves and material dislodging, evidently demonstrating both abrasive and delaminated wear. Al-bronze shows groves caused by hard particles that were enhanced in the abrading action (Fig. 16a). In the same wear environment, the microphotographs of trace Sc and Zr-added Al-bronze show small groves and plastic deformation, along with adhesion wear, as these elements' additions retained their strength at higher temperatures (Figs. 16b and 16c) [30, 46]. Additionally, high-magnification SEM microphotographs of the Al-bronze confirm that this type has coarse grains compared to finer grains of the bronze refined with trace amounts of Sc and Zr [5, 12]. Moreover, the high magnification micrographs reveal that the plastic deformation in the case of the Sc-added alloy is relatively

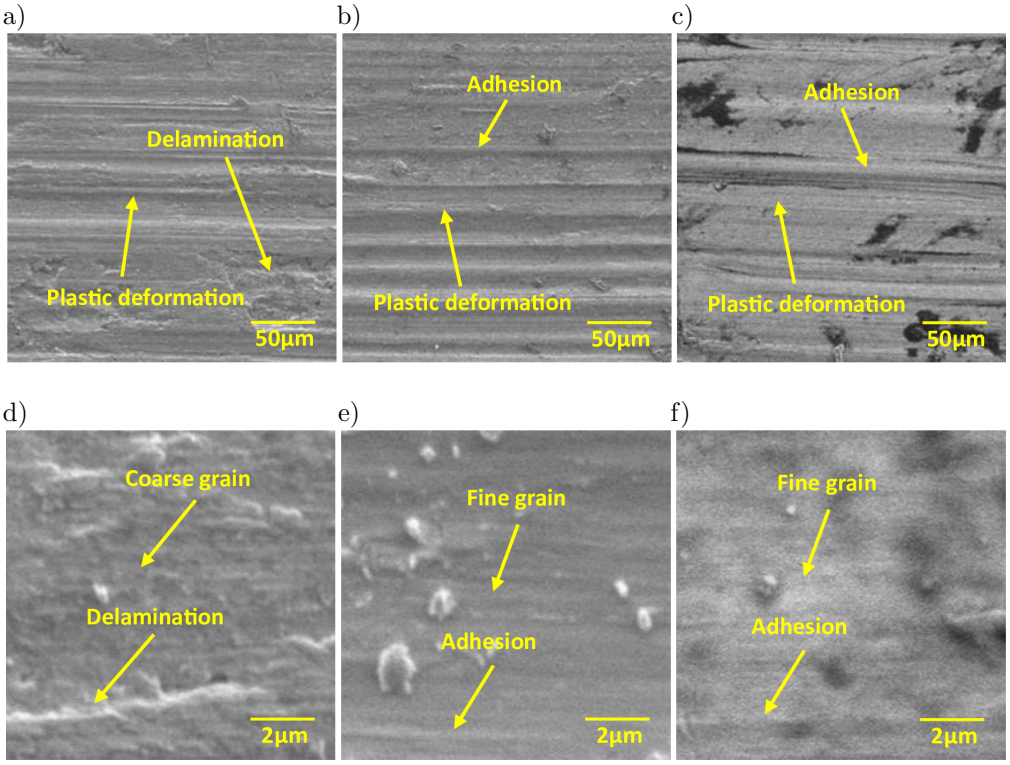

FIG. 16. SEM micrograph of worn surfaces after 3000 m of dry sliding at an applied pressure of 1.02 MPa: (a, d) Al-bronze, (b, e) trace Sc-added Al-bronze and (c, f) trace Zr-added Al-bronze.

low, indicating better strength compared to the Zr-added alloy. Furthermore, the highest distortion is observed on the surface of Al-bronze.

3.5. Surface roughness

A comparison is made based on the center line average surface roughness R_a of three types of Al-bronzes in different environments, including dry, fresh, and simulated seawater. Figure 17 includes these roughness results. At the initial stage, the surface roughness in terms of center line average of the polished pin sample of all three Al-bronzes was very similar, close to 0.22 μm. Since aluminum bronze is a relatively soft material, more wear marks are created on its surface than with the added-Zr alloy when sliding in a dry environment. Additionally, the Sc-added alloy produces the fewest wear marks, indicating optimum strength. The opposite phenomenon, however, is observed in wet sliding environments where Zr-added alloy's surface refinement causes greater damage than that of Sc-added alloy. Refined grains mean a comparatively higher number of grains as well as a higher grain boundary density assigned to them [47]. On the other hand, corrosion products, involving NaCl, are found on surfaces. So, under pressure and temperature, the surface becomes smoother. Therefore, the surface roughness in this corrosive environment is lower and depends entirely on the corrosive substances. More specifically, it displays the roughness of the corrosive product on the surface. The differences in surface roughness are created only due to corrosive attacks on the alloy surface. As a result, the differences of center line average surface roughness between alloys are minimal.

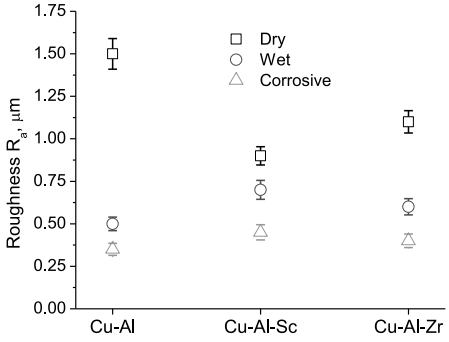

FIG. 17. Surface roughness of the worn surfaces under different sliding conditions.

4. SUMMARY AND CONCLUSIONS

This study looked into the friction as well as other properties of Al-bronze doped with trace amounts of Sc and Zr. The results lead to the following conclusions:

The addition of Zr improves tribological characteristics such as low specific wear rate and friction coefficient in the case of dry sliding, due to higher strength through grain refining and improved thermal stability. The addition of Sc further improves these properties through additional precipitation strengthening. However, in wet sliding environment and particularly in corrosive conditions, wear rates increase significantly compared to Al-bronze due to corrosion attack on the surface. The amount of dissolution of the corroded oxide film affects the rate of material wear. Scandium increases the intensity of the results since it accelerates the corrosion process.

Due to its superior strength, the friction coefficient of Sc-added alloy is lower than that of the Zr-added alloy followed by Al-bronze. This lack of friction coefficient may result from the material's low plastic deformation at the contact areas. However, in wet and corrosive environments, all friction coefficients decrease due to sealing effects in addition to the oxide layer being controlled. Optical microstructures also demonstrates that additions of Sc and Zr clearly refine the grains, strengthening the alloy.

In contrast to dry sliding conditions, visible wear tracks on worn surfaces are smoother in both wet and corrosive environments than in dry sliding conditions. This smoothness is attributed to the prevention of direct surface interactions and avoiding softening effect.

Because of thermal softening, Al-bronze has more abrasive wear on worn surfaces in dry sliding conditions. However, Sc and Zr additions clearly demonstrate the presence of fine particles on the worn surfaces, which improve the wear behavior.

The developed chips from the stainless-steel counter body show that the Sc-containing alloy produces the highest amount of chips, followed by the Zr-containing alloy, and then Al-bronze, in accordance with their respective degrees of hardness. The size of the chips produced by Al-bronze is largest followed by those produced by the bronze with Sc, and then the bronze with Zr, corresponding to their different degrees of grain refinement.

Acknowledgments

The author gratefully acknowledges the experimental facilities provided by the NCE Department of Bangladesh University of Technology, Dhaka, in addition to the DAERS Office, which were instrumental in conducting this study. Special thanks are extended to the Director of Administration for encouraging research activities at the International University of Business Agriculture and Technology, Dhaka.

References

1. Yang H.Y., Ma Z.C., Lei C.H., Meng L., Fang Y.T., Liu J.B., Wang H.T., High strength and high conductivity Cu alloys: A review, *Science China Technological Science*, **63**(12): 2505–2517, 2020, doi: 10.1007/s11431-020-1633-8.

2. Afifeh M., Hosseinipour S.J., Jamaati R., Manufacturing of pure copper with extraordinary strength-ductility-conductivity balance by cryorolling and annealing, *CIRP Journal of Manufacturing Science and Technology*, **37**: 623–632, 2022, doi: 10.1016/j.cirpj.2022.03.010.

3. Davis J.R., *Introduction and Overview of Copper and Copper Alloys, Metals Handbook, Desk Edition*, ASM International, Materials Park, Ohio, USA, 1998.

4. Shaik M.A., Golla B.R., Microstructure, mechanical and wear property correlation of Al bronze alloys, *Powder Metallurgy*, **66**(1): 54–63, 2023, doi: 10.1080/00325899.2022.2079183.

5. Haque M.S., Khan S.A.R., Kaiser M.S., Effect of Sc and Zr on precipitation behaviour of wrought Al-bronze, *IOP Conference Series: Materials Science and Engineering*, **1248**(012037): 1–12, 2022, doi: 10.1088/1757-899X/1248/1/012037.

6. Liu J., Liu J., Wang X., Study on phase transformation dynamics, microstructure, and properties of the Cu-2.7Ti-2.5-Ni-0.8V alloy, *Archives of Metallurgy and Materials*, **68**(4): 1383–1390, 2023, doi: 10.24425/amm.2023.146204.

7. Donatus U., Omotoyinbo J.A., Momoh I.M., Mechanical properties and microstructures of locally produced aluminium-bronze alloy, *Journal of Minerals and Materials Characterization and Engineering*, **11**(10): 1020–1026, 2012, doi: 10.4236/jmmce.2012.1110105.

8. Kaiser S., Kaiser M.S., Impact of cold plastic deformation and thermal post-treatment on the physical properties of copper based alloys Al-bronze and α-brass, *Acta Metallurgica Slovaca*, **27**(3): 114–121, 2021, doi: 10.36547/ams.27.3.951.

9. Koiwa M., Yamaguchi S., Hirabayashi M., Ageing characteristics of Cu-Be-Al alloys, *Transactions of the Japan Institute of Metals*, **8**(1): 62–69, 1967, doi: 10.2320/matertrans1960.8.62.

10. Totten G.E., *Heat Treating of Nonferrous Alloys*, ASM International, Vol. 4E, Materials Park, Ohio, USA, 2016.

11. Chen J., Wang J., Xiao X., Wang H., Chen H., Yang B., Contribution of Zr to strength and grain refinement in Cu-Cr-Zr alloy, *Materials Science and Engineering: A*, **756**: 464–473, 2019, doi: 10.1016/j.msea.2019.04.053.

12. Kaiser M.S., Ageing behaviour of minor Sc and Zr doped cast Cu-10Al Alloys, *International Journal of Engineering and Information Systems*, **3**(1): 7–14, 2019.

13. Suman P., Bannaravuri P.K., Baburao G., Kandavalli S.R., Alam S., Raju M.S., Pulisheru K.S., Integrity on properties of Cu-based composites with the addition of reinforcement: A review, *Materials Today: Proceedings*, **47**(19): 6609–6613, 2021, doi: 10.1016/j.matpr.2021.05.096.

14. Choudhry J., Larsson R., Almqvist A., A stress-state-dependent thermo-mechanical wear model for micro-scale contacts, *Lubricants*, **10**(9): 223, 2022, doi: 10.3390/lubricants10090223.

15. Akchurin A., Bosman R., Lugt P. M., van Drogen M., Analysis of wear particles formed in boundary-lubricated sliding contacts, *Tribology Letters*, **63**(2): 16, 2016, doi: 10.1007/s11249-016-0701-z.

16. Zmitrowicz A., Wear patterns and laws of wear – a review, *Journal of Theoretical and Applied Mechanics*, **44**(2): 219–253, 2006.

17. Soo V.K., Peeters J., Paraskevas D., Compston P., Doolan M., Duflou J.R., Sustainable aluminium recycling of end-of-life products: A joining techniques perspective, *Journal of Cleaner Production*, **178**: 119–132, 2018, doi: 10.1016/j.jclepro.2017.12.235.

18. Wu Z., Yuan W., Li J., Wang X., Liu L., Wang J., A critical review on the recycling of copper and precious metals from waste printed circuit boards using hydrometallurgy, *Frontiers of Environmental Science & Engineering*, **11**(5): 8, 2017, doi: 10.1007/s11783-017-0995-6.

19. ASTM G99-05, *Standard Test Method for Wear Testing with a Pin-on-Disk Apparatus*, American Society for Testing and Materials, West Conshohocken, Pennsylvania, USA, 2010.

20. Rahman M.M., Akash S.N., Afreen M., Ahmed S.R., Kaiser M.S., Tribological behavior of Sn-doped Cu under varied sliding environments, *6th International Conference on Mechanical, Industrial and Energy Engineering 'ICMIEE'*, Khulna, Bangladesh, December 19–21, 2020.

21. Cai W., Bellon P., Effect of annealing treatment on the dry sliding wear behavior of copper, *Wear*, **426–427**(Part B): 1187–1194, 2019, doi: 10.1016/j.wear.2019.01.014.

22. Equey S., Houriet A., Mischler S., Wear and frictional mechanisms of copper-based bearing alloys, *Wear*, **273**(1), 9–16, 2011, doi: 10.1016/j.wear.2011.03.030.

23. Liu P.F., Miao L., Deng Z., Zhou J., Gu Y., Chen S., Cai H., Sun L., Tanemura S., Flame-treated and fast-assembled foam system for direct solar steam generation and non-plugging high salinity desalination with self-cleaning effect, *Applied Energy*, **241**: 652–665, 2019, doi: 10.1016/j.apenergy.2019.02.030.

24. Khan A.A., Kaiser M.S., Role of silicon on the tribological performance of Al-based automotive alloys and the effect of used motor oil, *Tribologia – Finnish Journal of Tribology*, **39**(3–4): 12–20, 2022, doi: 10.30678/fjt.120669.

25. Ying D.Y., Zhang D. L., Solid-state reactions between Cu and Al during mechanical alloying and heat treatment, *Journal of Alloys and Compounds*, **311**(2): 275–282, 2000, doi: 10.1016/S0925-8388(00)01094-X.

26. Tian Y., Hang C., Wang C., Zhou Y., Evolution of Cu/Al intermetallic compounds in the copper bump bonds during aging process, *8th International Conference on Electronic Packaging Technology*, Shanghai, China, pp. 1–5, August 14, 2007, doi: 10.1109/ICEPT.2007.4441444.

27. Dvořák J., Král P., Kvapilová M., Svoboda M., Skleničk a V., Microstructure stability and creep behaviour of a Cu-0.2wt.%Zr alloy processed by equal-channel angular pressing, *Materials Science Forum*, **667–679**: 821–826, 2010, doi: 10.4028/www.scientific.net/MSF.667-669.821.

28. Bo H., Liu L.B., Jin Z.P., Thermodynamic analysis of Al-Sc, Cu-Sc and Al-Cu-Sc system, *Journal of Alloys and Compounds*, **490**(1–2): 318–325, 2010, doi: 10.1016/j.jallcom.2009.10.003.

29. Kaiser M.S., Sabbir S.H., Kabir M.S., Soummo M.R., Nur M.A., Study of mechanical and wear behaviour of hyper-eutectic Al-Si automotive alloy through Fe, Ni and Cr addition, *Materials Research*, **21**(4): e20171096, 2018, doi: 10.1590/1980-5373-MR-2017-1096.

30. Prabhudev M.S., Auradi V., Venkateswarlu K., Siddalingswamy N.H., Kori S.A., Influence of Cu addition on dry sliding wear behaviour of A356 alloy, *Procedia Engineering*, **97**: 1361–1367, 2014, doi: 10.1016/j.proeng.2014.12.417.

31. Archard J.F., Contact and rubbing of flat surfaces, *Journal of Applied Physics*, **24** (8): 981–988, 1953, doi: 10.1063/1.1721448.

32. Kaiser S., Kaiser M.S., Wear behavior of commercial pure copper with Al and Zn under dry, wet and corrosive environment, *Journal of Materials and Environmental Sciences*, **11**(4): 551–563, 2020.

33. Zhang X., Zhou X., Hashimoto T., Lindsay J., Ciuca O., Luo C., Sun Z., Zhang X., Tang Z., The influence of grain structure on the corrosion behaviour of 2A97-T3 Al-Cu-Li alloy, *Corrosion Science*, **116**: 14–21, 2017, doi: 10.1016/j.corsci.2016.12.005.

34. Shi Y., Pan Q., Li M., Huang X., Li B., Effect of Sc and Zr additions on corrosion behaviour of Al–Zn–Mg–Cu alloys, *Journal of Alloys and Compounds*, **612**: 42–50, 2014, doi: 10.1016/j.jallcom.2014.05.128.

35. Kaiser S., Kaiser M.S., A comparative study of chemical and physical properties of copper and copper alloys affected by acidic, alkaline and saline environments, *Journal of Electrochemical Science and Engineering*, **10**(4): 373–384, 2020, doi: 10.5599/jese.877.

36. Dhanasekaran S., Gnanamoorthy R., Dry sliding friction and wear characteristics of Fe-C-Cu alloy containing molybdenum di sulphide, *Materials and Design*, **28**(4): 1135–1141, 2007, doi: 10.1016/j.matdes.2006.01.030.

37. Meyer W.E., Walter J.D., *Frictional Interaction of Tire and Pavement, STP 793*, American Society for Testing and Materials, USA. 1983.

38. Moore A.J.W., Tegart W.J.M., Relation between friction and hardness, *Proceedings of the Royal Society of London. Series A, Mathematical and Physical Sciences*, **212**(1111): 452–458, 1952, doi: 10.1098/rspa.1952.0234.

39. Tyagi R., Xiong D., Li J., Effect of load and sliding speed on friction and wear behavior of silver/h-BN containing Ni-base P/M composites, *Wear*, **270**(7–8): 423–430, 2011, doi: 10.1016/j.wear.2010.08.013.

40. Zmitrowicz A., Wear debris: A review of properties and constitutive models, *Journal of Theoretical and Applied Mechanics*, **43**(1): 3–35. 2005.

41. Chen M., Shi X.H., Yang H., Liaw P.K., Gao M.C., Hawk J.A., Qiao J., Wear behavior of Al0.6CoCrFeNi high-entropy alloys: Effect of environments, *Journal of Materials Research*, **33**(19): 3310–3320, 2018, doi: 10.1557/jmr.2018.279.

42. Khan A.A., Kaiser M.S., Wear studies on Al-Si automotive alloy under dry, fresh and used engine oil sliding environment, *Research on Engineering Structures and Materials*, **9**(1): 1–18, 2023, doi: 10.17515/resm2022.505ma0816.

43. Song Q.N., Zheng Y.G., Ni D.R, Ma Z.Y., Studies of the nobility of phases using scanning Kelvin probe microscopy and its relationship to corrosion behaviour of Ni-Al bronze in chloride media, *Corrosion Science*, **92**: 95–103, 2015, doi: 10.1016/j.corsci.2014.11.039.

44. Bhuniya A.K., Chattopadhyay P.P., Datta S., Banerjee M.K., Study on the effect of trace zirconium addition on the microstructural evolution in Cu-Zn-Al shape memory alloy, *Materials Science and Engineering: A*, **391**(1–2): 34–42, 2005, doi: 10.1016/j.msea.2004.09.063.

45. Yu A.W., Yang C.G., Wang S.L., Liu F.C., Zheng Q., Effect of Sc, Zr grain refiner on the microstructure and mechanical properties of pure aluminum, *Applied Mechanics and Materials*, **508**: 16–21, 2014, doi: 10.4028/www.scientific.net/amm.508.16.

46. Rahman M.M., Ahmed S.R., Dry sliding friction and wear resistance of SnPb-solder affected copper against stainless steel counter surface, *Iranian Journal of Materials Science and Engineering*, **18**(4): 1–12, 2021, doi: 10.22068/ijmse.2334.

47. Wang P., Wang Y., Cui F., Yang X., Pan A., Wu W., Microstructural evolution, mechanical properties and corrosion resistance of CoCrFeNiW0.5 high entropy alloys with various annealing heat treatment, *Journal of Alloys and Compounds*, **918**: 165602, 2022, doi: 10.1016/j.jallcom.2022.165602.

Received March 25, 2024; accepted version May 16, 2024.
Online first July 2, 2024.